On the secular decay of the LARES semi-major axis

C. Pardini[a*], L. Anselmo[a], D.M. Lucchesi[a,b,c] and R. Peron[b,c]

[a] *Space Flight Dynamics Laboratory, Istituto di Scienza e Tecnologie dell'Informazione (ISTI), Consiglio Nazionale delle Ricerche (CNR) – Pisa, Italy*
[b] *Experimental Gravitation Section, Istituto di Astrofisica e Planetologia Spaziali (IAPS), Istituto Nazionale di Astrofisica (INAF) – Roma, Italy*
[c] *Istituto Nazionale di Fisica Nucleare (INFN), Sezione di Roma Tor Vergata, Via della Ricerca Scientifica 1 – Roma, Italy*

[*] *Corresponding author. Tel.: +39-050-315-2987; Fax: +39-050-315-2040;*
Postal address: ISTI/CNR, Via G. Moruzzi 1, 56124, Pisa, Italy;
E-mail: carmen.pardini@isti.cnr.it

Abstract

The laser-ranged satellite LARES is expected to provide new refined measurements of relativistic physics, as well as significant contributions to space geodesy and geophysics. The very low area-to-mass ratio of this passive and extremely dense satellite was chosen to reduce as much as possible the disturbing effects of non-gravitational perturbations. However, because of its height, about 1450 km compared with about 5800-5900 km for the two LAGEOS satellites, LARES is exposed to a much stronger drag due to neutral atmosphere.

From a precise orbit determination, analyzing the laser ranging normal points of LARES over a time span of about 3.7 years with the GEODYN II (NASA/GSFC) code, it was found an average semi-major axis decay rate of –0.999 m per year, corresponding to a non-conservative net force acting nearly opposite to the velocity vector of the satellite and with a mean along-track acceleration of -1.444×10^{-11} m/s^2.

By means of a modified version of the SATRAP (ISTI/CNR) code, the neutral drag perturbation acting on LARES was evaluated over the same time span, taking into account the real evolution of solar and geomagnetic activities, with five thermospheric density models (JR-71, MSIS-86, MSISE-90, NRLMSISE-00 and GOST-2004). All of them provided consistent results, well within their acknowledged uncertainties. Moreover, when the same models (JR-71 and MSIS-86) were used within GEODYN II in a least-square fit of the tracking data, the differences between the average drag coefficients estimated with SATRAP and GEODYN were of the order of 1% or less.

Unlike what happened for the two LAGEOS, where Yarkovsky thermal drag and charged particle drag were the leading causes, it was found that neutral atmosphere drag alone was able to explain most (≈98.6%) of the observed semi-major axis decay of LARES. The remaining ≈1.4%, corresponding to an average along-track acceleration of about -2×10^{-13} m/s^2 (i.e. ≈1/70 of neutral drag), was probably linked to thermal thrust effects. It was 50%, or less, of the value previously reported in the literature, but further and more detailed investigations, including the detection of the signature of the periodic terms, will be needed in order to characterize such smaller non-gravitational perturbation.

Keywords

LARES satellite; LARASE experiment; Neutral atmosphere drag; Satellite orbital decay; Non-gravitational perturbations.

1. Introduction

The LAser Ranged Satellites Experiment (LARASE) [1] has the goal to carry out a sequence of measurements of relativistic effects using specific Earth-orbiting satellites for verifying the predictions of General Relativity [2] and of alternatives theories proposed for the description of the gravitational interaction [3]. These measurements are achieved in the so-called weak-field and slow-motion (WFSM) limit of the theory, by means of passive "cannonball" satellites tracked very precisely with the Satellite Laser Ranging (SLR) technique through the International Laser Ranging Service (ILRS) [4].

The three satellites used in the LARASE experiment were chosen for the very good quality of their orbit determination, for the smallness of non-gravitational perturbations and for the accuracy of the dynamical model. They are the twin LAser GEOdynamics Satellites (LAGEOS and LAGEOS II), launched, respectively, in 1976 and in 1992, and LARES (LAser RElativity Satellite). LARES was launched from Kourou, in French Guiana, on 13 February 2012, with the qualification flight of the VEGA launcher. With a radius of 18.2 cm and a mass of 386.80 kg, this completely passive sphere, made of tungsten alloy and uniformly hosting on its surface 92 corner cube laser retro-reflectors, is the densest object in orbit in the Solar System, with an area-to-mass ratio $A/M = 2.69 \times 10^{-4}$ m^2/kg [5,6]. Placed into a nearly circular orbit at a mean geodetic altitude of about 1454 km and with an inclination of 69.5°, LARES was conceived with the goal of measuring the Lense-Thirring effect induced by the rotating mass of the Earth and predicted by General Relativity [7,8] with an accuracy of the order of 1% [5].

The scientific objectives of the LARES mission are therefore very ambitious. Certainly, the achievement of these objectives would be facilitated if, besides the high quality of the laser tracking of the satellite and its extremely low value for the area-to-mass ratio, it were possible to improve the dynamical models describing its motion, and that of the LAGEOS satellites, particularly concerning the subtle effects of non-gravitational perturbations [1,9]. Among these, the effects of the neutral atmosphere drag deserve a special attention in the case of LARES, the satellite having been placed in a relatively low orbit, where the residual Earth atmosphere cannot be ignored, compared with other perturbations whose modeling is relevant for meeting the scientific goals of the mission.

The reliable and detailed estimation of the perturbing accelerations induced on the LARES satellite by neutral atmosphere drag is therefore the main purpose of this paper, offering new insights on other non-gravitational perturbations, e.g. charged particle and thermal drag. The rest of the paper is organized as follows. In Section 2, we focus on the decay we observed for the semi-major axis of LARES after a precise orbit determination and on the corresponding deceleration we can infer along the transverse direction. In Sections 3 and 4, we describe the neutral atmosphere experienced by LARES, the role of the satellite drag coefficient and the detailed modeling of neutral drag on LARES on the basis of five atmospheric density models. In Section 5, we show the results of a new precise orbit determination once the neutral drag is modeled, highlighting anyway the presence of a residual very small deceleration not explainable in terms of the perturbing effects due to the neutral drag atmosphere. Finally, in Section 5, our conclusions and recommendations are provided.

2. The observed orbital decay of LARES

In order to reduce as much as possible the effects of the non-gravitational perturbations, LARES was designed and built with an area-to-mass ratio 2.6 times smaller than that of the twin LAGEOS and LAGEOS II satellites, placed at mean geodetic altitudes, respectively, of 5897 km and 5785 km. Compared with the two LAGEOS, this led, in fact, to smaller direct solar radiation pressure (the largest non-gravitational acceleration on LARES), Earth radiation pressure and thermal re-radiation [1,10]. However, due to the significantly lower altitude of LARES, neutral atmosphere drag was expected to be approximately 50 times stronger than for the two LAGEOS [1]. The accurate understanding and modeling of such non-gravitational perturbation is therefore of paramount importance for LARES if the ambitious scientific goals of the mission have to be met in a credible way.

Analyzing the laser ranging data available since the satellite launch, in February 2012, up to mid-2014, an average semi-major axis decay $\Delta a = -1.17$ m per year was reported [10]. In order to check these preliminary results, we carried out a Precise Orbit Determination (POD), based on the LARES laser ranging data (normal points) acquired by the ILRS from 6 April 2012 to 25 December 2015. The analysis was performed with the NASA/GSFC software package GEODYN II [11,12], fitting the observables over 7-day orbit arcs and not including in the dynamical model neither the neutral and charged atmospheric drag, nor any thermal effect. In this way, the detailed secular decrease of the LARES semi-major axis was uncovered, over more than 3.7 years (Figure 1). The corresponding average value found was $\Delta a = -0.999$ m per year [13,14].

Despite the apparent smallness of the measured decay, its relatively stable secular trend allows the detection of the semi-major axis decrease even using orbit determinations much more inaccurate than those obtained with laser ranging normal points. In fact, in a totally independent analysis, we used the two-line elements sets [15,16] determined by the US Strategic Command over 3.7 years, from 18 February 2012 to 22 October 2015, revealing an average secular $\Delta a = -0.952$ m per year. Therefore, during the first 3.7 years in orbit, LARES was subjected to an average semi-major axis decay of 2.7 mm per day, and these results indicate that a non-conservative net force was acting on the satellite, with a mean along-track acceleration component $\langle T \rangle = -1.444 \times 10^{-11}$ m/s^2.

It is worth remembering that in the case of LAGEOS [17], and later on of LAGEOS II, the detection of a small (and originally unexplained) $\Delta a = -0.402$ m per year (in 1994-2011 the semi-major axis decay settled to, on average, $\Delta a = -0.203$ m per year for LAGEOS and $\Delta a = -0.239$ m per year for LAGEOS II [18]) lead to an extensive physical investigation and modeling effort, for assessing and evaluating the potential effects of several non-gravitational perturbations [19-30]. Consequently, it was quite logical to investigate the similarities and differences among the LARES and LAGEOS satellites semi-major axis decay, as a first step to characterize, quantify and properly model the non-gravitational perturbations acting on the former, in particular taking into account that the non-gravitational mean along-track acceleration acting on LARES is currently nearly 5 times larger than those acting on the two LAGEOS satellites.

It was known since the beginning of the 1980's [19-21] that neutral atmosphere drag was not able to account for the LAGEOS orbital decay, being one order of magnitude too small (~14%, according to [28]). Yarkovsky thermal drag (~70%) and charged particle drag (~16%) were the dominant causes [28]. However, the considerably lower altitude of LARES put the attention on neutral atmosphere drag as the leading cause of the observed secular decrease of the semi-major axis, as even simple analytical computations were able to suggest.

In fact, assuming a circular orbit (the LARES eccentricity is less than 10^{-3}) and that all the observed semi-major decay was due to neutral atmosphere drag, the average neutral atmospheric density ρ at the satellite altitude could be estimated as follows:

$$\rho = -\Delta a_{\mathrm{rev}} / [2\pi (C_{\mathrm{D}} \cdot A/M) a^2] \qquad (1)$$

where C_D is the so-called drag coefficient, defined in Section 3, a is the semi-major axis, and Δa_{rev} represents its variation over one revolution [31]:

$$\Delta a_{rev} = -2\pi(C_D \cdot A/M)\rho a^2 \quad (2)$$

Taking into account that the LARES orbital period is about 6885 s and that during 1300 days the semi-major axis decreased by about −3.5 m (Figure 1), the average Δa_{rev} resulted to be -2.15×10^{-4} m per revolution. Substituting this value of Δa_{rev} in Eq. (1), together with a = 7820.2 km and C_D = 3.5 (a reasonable pre-launch guess), it was then possible to estimate the mean neutral atmosphere density, at the LARES altitude, needed to explain the observed semi-major axis decay. The value obtained was $\rho = 5.9 \times 10^{-16}$ kg/m^3.

For LARES the estimated density was not one order of magnitude greater than what should have been expected, as happened for the LAGEOS satellites, but was instead in sound agreement with the predictions of thermospheric density models. For instance, assuming the Jacchia 1971 model [32], at the altitude of LARES it predicted an average neutral density $\langle\rho\rangle = 3.48 \times 10^{-16}$ kg/m^3 with an exospheric temperature T_∞ = 500 K, $\langle\rho\rangle = 6.32 \times 10^{-16}$ kg/m^3 with T_∞ = 1000 K, and $\langle\rho\rangle = 1.20 \times 10^{-14}$ kg/m^3 with T_∞ = 2000 K. Therefore, even a very rough and preliminary estimation seemed to indicate that, considering the appropriate environmental conditions (i.e. solar and geomagnetic activities) prevailing during the time interval considered, characterized by $\langle T_\infty\rangle$ = 971 K, neutral atmosphere drag was able to explain most of the observed orbital decay. Therefore, its effects on LARES were investigated in detail and the results obtained are presented in this paper.

3. Neutral atmosphere drag

Atmospheric drag is the largest non-gravitational perturbation acting on satellites below the altitude of ~1000 km [33], and also at the LARES altitude must be taken into account to explain the details of the orbital evolution inferred from the extremely accurate tracking made possible by laser ranging. The most revealing feature of the drag force, which for a spherical body with uniform surface properties is directed opposite to the satellite's velocity relative to the atmosphere, is the dissipation of orbital energy, leading to a gradual decrease of the satellite's semi-major axis.

It is usual to express the drag force ($\vec{F}_D$) in the form:

$$\vec{F}_D = M\vec{a}_D = -\frac{1}{2}\rho C_D A V_r^2 \frac{\vec{V}_r}{V_r} \quad (3)$$

in which $\vec{a}_D$ is the corresponding acceleration, M is the mass of the satellite, ρ is the local atmospheric density, $\vec{V}_r$ is the velocity of the satellite relative to the atmosphere, A is the cross-sectional area of the satellite facing the airstream, and C_D is the drag coefficient, i.e. a dimensionless quantity which summarizes the interaction of the atmospheric molecules with the surface of the satellite exposed to the flow [32,33]. The values of the area and the mass are well known in the case of LARES, but the relative velocity, which depends on the complex dynamics of the Earth's atmosphere, may be affected by uncertainties larger than 1%. However, a reasonable approximation of $\vec{V}_r$ is obtained with the assumption that the atmosphere co-rotates with the Earth, i.e.:

$$\vec{V}_r = \vec{V} - \vec{\omega}_\oplus \times \vec{r} \quad (4)$$

where $\vec{V}$ is the satellite inertial velocity, $\vec{r}$ its position vector, and $\vec{\omega}_{\oplus}$ is the Earth's angular velocity vector. In most situations this assumption leads to negligible errors, but during the relatively short duration (from several hours to a few days) of major geomagnetic storms, occurring approximately 5% of the time, the atmospheric winds may grow remarkably [34].

In general, however, the drag coefficient and the atmospheric density represent the principal causes of uncertainty in computing the drag force. This is the consequence of the fact that when $\vec{F}_{\mathrm{D}}$ or $\vec{a}_{\mathrm{D}}$ are measured, for instance through the observed orbital decay of a satellite, it is the product $\rho \cdot C_{\mathrm{D}}$ which is determined, so any uncertainty in C_{D} brings forth an uncertainty in the air density ρ, and vice versa. Therefore, for this and other reasons [35], any semi-empirical atmospheric density model may be affected by significant errors. Nevertheless, if Eqs. (3) and (4) rightly fit the behavior of the drag force and the air density ρ is appropriately described by a sufficiently sophisticated model, i.e. able to follow the changes induced by the varying solar and geomagnetic activity and by seasonal effects, a large fraction of the uncertainty in ρ, as well as other possible and smaller contributions from other perturbations having the same signature of neutral drag, might be incorporated in the value of C_{D}, if set as solve for parameter in the precise orbit determination process. In other words, the value of C_{D} so determined would not necessarily correspond to the physical aerodynamic drag coefficient of the satellite, having to absorb the average density bias of the atmospheric model, during the considered integration arc, and other possible smaller drag-like influences (limited to the constant component, if C_{D} were assumed constant as well over the integration arc). However, such a procedure would lead in any case to a better orbit determination and to smaller residuals, benefitting the primary goal of the mission, i.e. the General Relativity measurements.

Of course, if the aim of the measurements were the precise and accurate determination of air density as a function of the season and space weather conditions, an independent estimation of the physical drag coefficient would be needed, to be compared with the C_{D} found as solve for parameter in the precise orbit determination process [35]. Nevertheless, as explained above, this was not necessary for the primary goals of the LARASE experiment and was not among the purposes of this paper.

4. Detailed modeling of the neutral atmosphere drag on LARES

In view of the central role played by neutral atmosphere drag among the non-gravitational forces acting on LARES, a detailed modeling of such perturbation was deemed necessary for a better characterization and estimation of the other non-gravitational forces, and for the success of the LARASE experiment. To do so, a modified version of the SATRAP tool, developed at ISTI/CNR [35,36], was used to model the neutral drag acceleration acting on LARES, as a function of time, taking into account the real evolution of solar and geomagnetic activities and the observed mean secular along-track acceleration. In fact, many atmospheric density models have been implemented in SATRAP over more than 20 years of development, including Jacchia-Roberts 1971 (JR-71) [37], the Mass Spectrometer and Incoherent Scatter radar 1986 model (MSIS-86) [38], the Mass Spectrometer and Incoherent Scatter radar Extended 1990 (MSISE-90) [39], NRLMSISE-00 [40,41], developed at the US Naval Research Laboratory (NRL), GOST-2004 [42], issued by the State Committee on Standardization and Metrology of the Russian Federation, and Jacchia-Bowman 2008 (JB2008) [43].

All the above mentioned thermospheric density models were used within SATRAP to compute the components of the neutral drag acceleration on LARES in the reference system *RTW* [44], having the origin in the center of mass of the satellite and with three orthogonal axes aligned, respectively, along the radial direction, from the center of the Earth to the satellite ($\vec{R}$), normal to

the orbit plane, in the direction of the osculating orbital angular momentum ($\vec{W}$), and in the transverse (along-track) direction ($\vec{T}$), lying on the orbital plane 90 degrees from $\vec{R}$, nearly aligned with the satellite velocity vector. This analysis covered the first 3.7 years, from 6 April 2012 to 25 December 2015, and the drag coefficients C_D were rescaled in order to reproduce, with each atmospheric density model, the observed average transverse acceleration component $\langle T \rangle = -1.444 \times 10^{-11}$ m/s^2. For the applicable time interval, Figure 2 shows the geodetic altitude, the exospheric temperature and the overall atmospheric density, while Figure 3 shows the concentration of the three main atomic species, i.e. helium (He), hydrogen (H) and oxygen (O). Both figures were obtained with NRLMSISE-00.

Concerning the JB2008 model, the results obtained were not presented in this paper for the following reason. Contrary to the other models, where only one solar and one geomagnetic index are used (both based on ground measurements), JB2008 employs four solar and two geomagnetic indices (some based on satellite measurements), and the process of obtaining and validating them is much more lengthy and complicated [45]. Specifically concerning the time interval covered in our analysis, i.e. the first 3.7 years of LARES, different releases of such parameters, in particular of the S10 index, presented significant changes. This was due to degradations in some spacecraft sensors used to create S10 since 2010, needing updated corrections [46]. As a consequence, with the indices release of 15 April 2016, the average drag coefficient obtained was $\langle C_D \rangle = 3.50$, while, with the release of 14 December 2016, $\langle C_D \rangle = 3.03$. Having not a direct control on the calibration process of the indices and waiting for a reliable validation of their estimates, it was therefore decided to exclude the JB2008 results from this paper, with the intention to include them in successive analyses. Moreover, being JB2008 not included in the GEODYN II code used for the precise orbit determinations of the LARASE experiment, there were, in any case, no adverse impacts on the purposes of the present work.

The results obtained with all the other models are summarized in Figures 4 and 5, and in Table 1. In order to fit the mean secular along-track non-gravitational acceleration $\langle T \rangle$ measured on LARES, the various thermospheric density models converged, as expected, to different average drag coefficients, from $\langle C_D \rangle = 3.71$ in the case of MSIS-86 to $\langle C_D \rangle = 4.21$ in the case of GOST-2004 (Table 1). The mean value was $\langle C_D \rangle = 3.88$, with a maximum discrepancy of +8.5% for the Russian model. However, considering that NRLMSISE-00 was a refinement of MSIS-86 and MSISE-90, sharing with them a common heritage, the mean among the three more independent thermospheric models JR-71, NRLMSISE-00 and GOST-2004 was $\langle C_D \rangle = 3.98$, with a maximum discrepancy of +5.8% for GOST-2004. The mean biases among the models, up to ~9% (~6%, if only the last three independent models are considered) with respect to the averaged values and up to ~13% among the models themselves, are not surprising, because they are fully consistent with their known uncertainties [47-49], and with the fact that all thermospheric density models, including those analyzed in this study, were developed using data coming from much lower altitudes and validated there. The performances exhibited at the LARES altitude can be therefore considered quite satisfactory, and also rather old models still widely used, like JR-71 and MSIS-86, were able to reproduce extremely well, with a small $\langle C_D \rangle$ rescaling by +4.5% and −1.9%, respectively, the behavior of a CIRA-2012 standard model like NRLMSISE-00 [49].

More specifically, MSIS-86, MSISE-90 and NRLMSISE-00 shared the same signature, with a very good agreement in terms of T magnitude and time evolution, with lower peaks exceeding -5×10^{-11} m/s^2. JR-71 still displayed a relatively good agreement with the T signature of the other three models, but with deeper lower peaks, sometimes exceeding -6×10^{-11} m/s^2. The Russian model GOST-2004, however, behaved differently, presenting a quite distinct signature and smaller magnitude excursions of T, with a value nearly always higher than -3×10^{-11} m/s^2.

Even though less relevant in the context of the LARES semi-major axis decay, the other components of the neutral drag acceleration were also estimated. As an example, Figure 6 shows the results obtained with NRLMSISE-00. First of all, it should be mentioned that the radial R and

normal W components resulted to have, as expected, mean values close to zero, together with short and long-term oscillations quite smaller than the transverse component T. Again, there was a very good agreement among the time evolution signatures of MSIS-86, MSISE-90 and NRLMSISE-00, and, to a slightly lesser extent, of JR-71, with the radial component R mostly varying between $\pm 4.5 \times 10^{-14}$ m/s^2 and the normal component W mostly varying between $\pm 2.6 \times 10^{-12}$ m/s^2. GOST-2004 presented similar magnitude excursions, just a little bit smaller in the extreme values, but, as in case of the T component, the time evolution signature was distinctly different with respect to the other models considered, as shown in Figure 7.

5. LARES precise orbit determination including neutral atmosphere drag

Having investigated the perturbing acceleration due to neutral atmosphere drag acting on LARES, the GEODYN II code was used to obtain a precise orbit determination including such perturbation. The force model incorporated the EIGEN-GRACE02S static model for the Earth's gravity field [50], direct solar radiation pressure with eclipses [12], the Earth's albedo [26], and the time-varying components of the geopotential [51,52].

Among the three neutral atmosphere models implemented in GEODYN, two, i.e. JR-71 and MSIS-86, had been also investigated with SATRAP and were then chosen for the precise orbit determination runs. Based on the results outlined in the previous section, MSIS-86 was very similar to the CIRA-2012 standard NRLMISE-90, but the overall behavior of JR-71 was anyway highly coherent with that of the other American models, sharing a common development history and some data sets, provided that the drag coefficient were appropriately rescaled. According to the results obtained, both JR-71 and MSIS-86 can be therefore considered validated and appropriate for the LARES orbit determination with GEODYN II, delivering a description of the neutral drag perturbation consistent with the predictions, uncertainties and range of applicability of all the thermospheric density models analyzed.

As in the case, mentioned at the beginning, in which atmospheric drag was not included in the dynamical model, GEODYN II was again used to fit the observables over 7-day orbit arcs, from 6 April 2012 to 25 December 2015, using either JR-71 or MSIS-86. The effect on the semi-major axis residuals was dramatic, as shown in Figure 8, with a nearly complete cancellation. This result was obtained by JR-71 with $\langle C_D \rangle = 3.96$, and by MSIS-86 with $\langle C_D \rangle = 3.76$, i.e. in extremely good agreement with the totally independent estimates carried out with SATRAP (Table 1). In the first case the difference was, in fact, +0.25%, in the second one +1.35%, confirming again that neutral atmosphere drag alone (or a combination of forces with exactly the same signature) can explain most of the observed semi-major axis decay of LARES.

However, it should also be stressed that, after modeling the neutral drag perturbation in GEODYN II, a residual semi-major axis decay was still present (see Figure 8), corresponding to an average transverse acceleration $\langle T_R \rangle = -2 \times 10^{-13}$ m/s^2, i.e. $\approx$1/70 of neutral drag. Probably, the thermal thrust effects came to play a role at this level, but the value found was only about 50%, or less, of that previously reported [53,54] and modeled [55-57], so further and more detailed investigations, including the detection of the signature of the periodic terms, will be needed for characterizing such smaller non-gravitational perturbations.

6. Conclusions

As we briefly mentioned in Section 1, LARASE [1] has as final goal a number of precise measurements of relativistic effects in the so-called WFSM limit of Einstein's General Relativity [3], in particular of the Lense-Thirring precession [7,8] of the orbit of the considered satellites, the two LAGEOS and LARES. However, a peculiarity of the LARASE activities and purposes is to

provide such precise measurements of gravitational effects with a very robust and reliable estimate of the systematic sources of error in such a way to build, for each measurement, a very accurate error budget [1,14]. These systematic errors are due to both gravitational and non-gravitational perturbations. Therefore, a consistent work within LARASE is devoted to improve current perturbative models, especially those related with the non-gravitational perturbations [9] and, among these, those dealing with thermal thrust effects. The work presented in this paper falls within these activities. In fact, before attacking the impact of unmodeled thermal perturbations on LARES, we need to fix the disturbing effects on the satellite orbit of the perturbations related with direct solar radiation pressure, Earth's albedo and – because of the relative low height of LARES – atmosphere neutral drag, indeed the main subject of this work.

Having the experience of the two LAGEOS in mind, LARES was conceived to minimize as much as possible the impact of non-gravitational perturbations on its precise orbit determination based on laser ranging measurements. The clever design was certainly successful in achieving the highest bulk density of any known orbiting object, either natural or man-made, in the Solar System, with a correspondingly very low value of the area-to-mass ratio. However, the relatively low orbit in which LARES was placed curtailed in part the advantages of a so low area-to-mass ratio. Indeed, while direct solar radiation pressure was smaller for LARES by a factor 2.6, the Earth's albedo radiation pressure was only slightly reduced, because of the lower height. The effects of thermal emissions were probably significantly abated as well, whereas for neutral atmosphere drag an increase of some tens of times was expected compared with the two LAGEOS.

The main goal of this study was indeed the accurate estimation of the neutral drag perturbation on LARES. It was found that neutral atmosphere drag alone was able to explain most (≈98.6%) of the observed semi-major axis decay of the satellite. All the adopted thermospheric density models provided consistent results, well within their acknowledged uncertainties, and when the same models were used both in SATRAP and GEODYN, the differences between the estimated average drag coefficients were of the order of 1% or less.

Finally, modeling the neutral atmosphere drag within GEODYN II, a residual semi-major axis decay of LARES, corresponding to an average along-track acceleration of about -2×10^{-13} m/s^2 (i.e. ≈ 1/70 of neutral drag), was detected as well. If linked to thermal emission effects, it was more than two orders of magnitude smaller than for the two LAGEOS, providing a striking demonstration of the LARES good design in terms of minimization of non-gravitational forces [53]. Again, also considering the predominant role played by neutral atmosphere drag, further and more detailed investigations, including the detection of the signature of the periodic terms, will be needed in order to characterize such smaller non-gravitational perturbations and disentangle them from other possible effects, like tiny anisotropic radiation reflection and charged particle drag.

In conclusion, the combination of satellite design and operational orbit choice resulted for LARES in an overturning of the impact of non-gravitational perturbations compared with the two LAGEOS satellites, putting neutral atmosphere drag at center stage. Any accurate analysis of the LARES orbit and any deep investigation of small forces effects cannot then ignore a thorough scrutiny of such an important perturbation.

Acknowledgements

This work was carried out in the framework of the LAser RAnged Satellites Experiment (LARASE) and was in part supported by the Commissione Scientifica Nazionale II (CSNII) on Astroparticle Physics Experiments of the Istituto Nazionale di Fisica Nucleare (INFN), in Italy.

The authors acknowledge the International Laser Ranging Service (ILRS) for providing high quality laser ranging data of the LARES satellite and the US Space Track Organization for making available the Two-Line Elements of LARES used in this study.

References

1. Lucchesi, D.M., Anselmo, L., Bassan, M., Pardini, C., Peron, R., Pucacco, G., Visco, M., Testing the gravitational interaction in the field of the Earth via satellite laser ranging and the laser ranged satellites experiment (LARASE), Classical Quantum Gravity 32 (2015), 155012 (50pp).
2. Einstein, A., Die Grundlage der allgemeinen Relativitätstheorie, Annalen der Physik 354 (1916) 769–822.
3. Will, C.M., Theory and experiment in gravitational physics, Cambridge University Press, Cambridge, United Kingdom, 1993 (see also: http://adsabs.harvard.edu/abs/2014LRR....17....4W).
4. Pearlman, M.R., Degnan, J.J., Bosworth, J.M., The international laser ranging service, Advances in Space Research 30 (2002) 135–143.
5. Ciufolini, I., Paolozzi, A., Pavlis, E.C., Ries, J.C., Koenig, R., Matzner, R.A., Sindoni, G., Neumayer, H., Towards a one percent measurement of frame dragging by spin with satellite laser ranging to LAGEOS, LAGEOS 2 and LARES and GRACE gravity models, Space Science Reviews 148 (2009) 71–104.
6. Paolozzi, A., Ciufolini, I., LARES successfully launched in orbit: Satellite and mission description, Acta Astronautica 91 (2013) 313–321.
7. Lense, J., Thirring, H., Über die Einfluß der Eigenrotation der Zentralkörper auf die Bewegung der Planeten und Monde nach der Einsteinschen Gravitationstheorie, Zeit. Phys. 19 (1918) 156–163.
8. Mashhoon, B., Hehl, F.W., Theiss, D.S., On the gravitational effects of rotating masses: The Thirring-Lense papers, Gen. Relativ. Gravit. 16 (1984) 711–750.
9. Visco, M., Lucchesi, D.M., Review and critical analysis of mass and moments of inertia of the LAGEOS and LAGEOS II satellites for the LARASE program, Advances in Space Research 57 (2016) 1928–1938.
10. Sośnica, K., Impact of the atmospheric drag on Starlette, Stella, Ajisai, and LARES orbits, Artificial Satellites 50 (2015) 1–18.
11. Putney, B., Kolenkiewicz, R., Smith, D., Dunn, P., Torrence, M.H., Precision orbit determination at the NASA Goddard Space Flight Center, Advances in Space Research 10 (1990) 197–203.
12. Pavlis, D.E., Luo, S., Dahiroc, P., McCarthy, J.J., Luthcke, S.B., GEODYN II operations manual, NASA/GSFC and STX Systems Corp., Greenbelt (MD), USA, 1998.
13. Lucchesi, D.M., Peron, R., Anselmo, L., Bassan, M., Magnafico, C., Nobili, A.M., Pardini, C., Pucacco, G., Stanga, R., Visco, M., Precise orbit determination of the two LAGEOS and LARES satellites and the LARASE activities, Geophysical Research Abstracts 18 (2016), Poster EGU2016-15626.
14. Lucchesi, D.M., Magnafico, C., Peron, R., Visco, M., Anselmo, L., Pardini, C., Bassan, M., Pucacco, G., Stanga, R., Measurements of General Relativity precessions in the field of the Earth with laser-ranges satellites and the LARASE program, in 2016 IEEE Metrology for Aerospace (MetroAeroSpace), June 2016, 522–529.
15. Hoots, F.R., Roehrich, R.L., Models for propagation of NORAD elements sets, Spacetrack Report No. 3, Project Spacetrack, Aerospace Defense Command, United States Air Force, Colorado Springs, CO, USA, 1980.
16. Vallado, D.A., Crawford, P., SGP4 orbit determination, In: 2008 AIAA/AAS Astrodynamics Specialist Conference, Honolulu, Hawaii, USA, Paper AIAA 2008-6770, 2008.
17. Smith, D.E., Dunn, P., Long term evolution of the LAGEOS orbit, Geophys. Res. Letters 7 (1980) 437–440.
18. Sośnica, K., Determination of precise satellite orbits and geodetic parameters using satellite laser ranging, Astronomical Institute, University of Bern, Switzerland, 2014, p. 205.

19. Rubincam, D.P., Atmospheric drag as the cause of the secular decrease in the semimajor axis of LAGEOS's orbit, Geophys. Res. Lett. 7 (1980) 468–470.
20. Afonso, G., Barlier, F., Berger, C., Mignard, F., Effet du freinage atmosphérique et de la traînée électrique sur la trajectoire du satellite LAGEOS, Comptes Rendus de l'Académie des Sciences 290B (1980) 445–448 (in French).
21. Rubincam, D.P., On the secular decrease in the semimajor axis of LAGEOS's orbit, Celestial Mechanics 26 (1982) 361–382.
22. Anselmo, L., Farinella, P., Milani, A., Nobili, A.M., Effects of the Earth-reflected sunlight on the orbit of the LAGEOS satellite, Astronomy and Astrophysics 117 (1983) 3–8.
23. Afonso, G., Barlier, F., Berger, C., Mignard, F., Walch, J.J., Reassessment of the charge and neutral drag of LAGEOS and its geophysical implications, J. Geophys. Res. 90B (1985) 9381–9398.
24. Rubincam, D.P., Weiss, N.R., The orbit of LAGEOS and solar eclipses, J. Geophys. Res. 90B (1985) 9399–9402.
25. Rubincam, D.P., Weiss, N.R., Earth albedo and the orbit of LAGEOS, Celestial Mechanics 38 (1986) 233–296.
26. Rubincam, D.P., Knocke, P., Taylor, V.R., Blackwell, S., Earth anisotropic reflection and the orbit of Lageos, J. Geophys. Res. 92B (1987) 11662–11668.
27. Rubincam, D.P., Yarkovsky thermal drag on LAGEOS, J. Geophys. Res. 93B (1988) 13805–13810.
28. Rubincam, D.P., Drag on the LAGEOS satellite, J. Geophys. Res. 95B (1990) 4881–4886.
29. Martin, C.F., Rubincam, D.P., Effects of Earth albedo on the LAGEOS I satellite, J. Geophys. Res. 101B (1996) 3215–3226.
30. Andrés de la Fuente, J.I., Enhanced modelling of LAGEOS non-gravitational perturbations, PhD Thesis, Delft University Press, Delft, The Netherlands, 2007.
31. Larson, W.J., Wertz, J.R., (Eds.), Space mission analysis and design, Second edition, Fourth printing, Kluwer Academic Publishers, Dordrecht/Boston/London, 1996, p. 143.
32. Zarrouati, O., Trajectoires spatiales, Cepadues Editions, Toulouse, France, 1987 (in French).
33. Montenbruck, O., Gill, E., Satellite orbits: models, methods, and applications, Springer, Berlin, Germany, 2001.
34. Moe, K., Moe, M.M., Rice, C.J., Simultaneous analysis of multi-instrument satellite measurements of atmospheric density, Journal of Spacecraft and Rockets 41 (2004) 849–853.
35. Pardini, C., Moe, K., Anselmo, L., Thermospheric density model biases at the 23rd sunspot maximum, Planetary and Space Science 67 (2012) 130–146.
36. Pardini, C., Anselmo, L., SATRAP: Satellite reentry analysis program, Internal Report C94-17, CNUCE Institute, Consiglio Nazionale delle Ricerche (CNR), Pisa, Italy, 1994.
37. Cappellari, J.O., Velez, C.E., Fuchs, A.J. (Eds.), Mathematical theory of the Goddard Trajectory Determination System, NASA/GSFC Report, GSFC X-582-76-77, Greenbelt, MD, USA, 1976, pp. 4-33–4-53.
38. Hedin, A.E., MSIS-86 thermospheric model, J. Geophys. Res. 92 (1987) 4649–4662.
39. Hedin, A.E., Extension of the MSIS thermosphere model into the middle and lower atmosphere, J. Geophys. Res. 96 (1991) 1159–1172.
40. Picone, J.M., Hedin, A.E., Drob, D.P., Lean, J., NRLMSISE-00 empirical model: comparisons to data and standard models, In: Astrodynamics 2001, Advances in the Astronautical Sciences Series, Vol. 109, Univelt Inc., San Diego (CA), USA, 2002, pp. 1385–1398.
41. Picone, J.M., Hedin, A.E., Drob, D.P., Aikan, A.C., NRLMSISE-00 empirical model of the atmosphere: Statistical comparisons and scientific issues, J. Geophys. Res. 107A12 (2002) 1468.
42. Volkov, I.I., Earth's upper atmosphere density model for ballistic support of the flight of artificial Earth satellites GOST R 25645.166-2004, Publishing House of the Standards, Moscow, 2004.

43. Bowman, B.R., Tobiska, W.K., Marcos, F.A., Huang, C.Y., Lin, C.S., Burke, W.J., A new empirical thermospheric density model JB2008 using new solar and geomagnetic indices, In: Proc. of AIAA/AAS Astrodynamics Specialist Conf. (18-21 August 2008, Honolulu, Hawaii), Paper AIAA 2008–6438, American Institute of Aeronautics and Astronautics, Reston (VA), USA, pp. 18–21.
44. Roy, A.E., Orbital motion, Third Edition, Adam Hilger, Bristol (UK) & Philadelphia (USA), 1988, pp. 191–192.
45. Tobiska, W.K., Bouwer, S.D., Bowman, B.R., The development of new solar indices for use in thermospheric density modeling, J. Atmos. Sol.-Terr. Phy. 70 (2008) 803–819.
46. Space Environment Technologies, The Jacchia-Bowman 2008 empirical thermospheric density model, URL: sol.spacenvironment.net/jb2008/, last accessed: 15 December 2016.
47. Volkov, I.I., Semenov, A.I., Suevalov, V.V., Analysis of thermospheric density variations neglected in modern atmospheric models using accelerometer data, Sol. Syst. Res. 42 (2008) 51–62.
48. Yurasov, V.S., Nazarenko, A.I., Cefola, P.J., Alfriend, K.T., Results and issues of atmospheric density corrections, In: 14th AAS/AIAA Space Flight Mechanics Meeting, Maui, Hawaii, USA, Paper AAS 04-305, 2004.
49. CIRA-2012 International Working Group, COSPAR International Reference Atmosphere 2012 (CIRA-2012) – Models of the Earth's upper atmosphere, Version 1.0, 31 July 2012.
50. Reigber, C., Schmidt, R., Flechtner, F., König, R., Meyer, U., Neumayer, K.H., Schwintzer, P., Zhu, S.Y., An Earth gravity field model complete to degree and order 150 from GRACE: EIGEN-GRACE02S, J. Geodyn. 39 (2005) 1–10.
51. Ray, R.D., A global ocean tide model from TOPEX/POSEIDON altimetry: GOT99.2, Technical Report NASA/TM-1999-209478, Goddard Space Flight Center (GSFC), Greenbelt (MD), USA, 1999.
52. Petit, G., Luzum, B. (Eds.), IERS conventions (2010), IERS Technical Note 36, Verlag des Bundesamts für Kartographie und Geodäsie, Frankfurt am Main, Germany, 2010.
53. Ciufolini, I., Paolozzi, A., Pavlis, E.C., Ries, J.C., Gurzadyan, V., Koenig, R., Matzner, R.A., Penrose, R., Sindoni, G., Testing General Relativity and gravitational physics using the LARES satellite, The European Physical Journal Plus, 127 (2012) 133(7).
54. Ciufolini, I., Paolozzi, A., Pavlis, E.C., Koenig, R., Ries, J.C., Gurzadyan, V., Matzner, R.A., Penrose, R., Sindoni, G., Paris, C., Preliminary orbital analysis of the LARES space experiment, The European Physical Journal Plus, 130 (2015) 133(5).
55. Nguyen, P.H., Matzner, R., Modelling LARES temperature distribution and thermal drag, The European Physical Journal Plus 130 (2015) 206(24).
56. Brooks, J.W., Matzner, R., Modelling LARES temperature distribution and thermal drag II: Numerical computation of current-epoch thermal forces, The European Physical Journal Plus 131 (2016) 222(11).
57. Matzner, R., Nguyen, P., Brooks, J., Ciufolini, I., Paolozzi, A., Pavlis, E.C., Koenig, R., Ries, J., Gurzadyan, V., Penrose, R., Sindoni, G., Paris, C., Khachatryan, H., Mirzoyan, S., LARES satellite thermal forces and a test of General Relativity, In: 3rd IEEE International Workshop on Metrology for Aerospace (MetroAeroSpace 2016) Proceedings, Institute of Electrical and Electronics Engineers (IEEE), Inc., Electronic ISBN: 978-1-4673-8292-2, 2016, pp. 516–521.

Figure captions

Figure 1. Semi-major axis decay of LARES determined by integrating the precise orbit estimation residuals over 3.7 years, obtained with GEODYN II not including in the dynamical model neither the neutral and charged atmosphere drag, nor the thermal effects.

Figure 2. LARES geodetic altitude, and ambient exospheric temperature and neutral atmosphere density, during the first 3.7 years of the mission. The exospheric temperature and the neutral atmosphere density were estimated with the NRLMSISE-00 empirical thermospheric model. The mean values were 1454 km for the geodetic altitude, 971.2 K for the exospheric temperature and 5.886×10^{-16} kg/m^3 for the neutral atmosphere density.

Figure 3. Concentrations of the main neutral atomic species (He, H and O) at the LARES altitude during the first 3.7 years of the mission. They were estimated with the NRLMSISE-00 empirical thermospheric model.

Figure 4. Transverse acceleration component (*T*) due to neutral drag acting on LARES, compared with the daily and 81-day average solar flux at 10.7 cm, and with the geomagnetic activity index K_p. The gray vertical belts in the first plot identify the eclipse periods, when the LARES orbit crossed the Earth's shadow.

Figure 5. Comparison of the transverse acceleration components due to neutral drag, as computed with the five models JR-71, MSIS-86, MSISE-90, NRLMSISE-00 and GOST-2004. The gray vertical belts identify the eclipse periods, when the LARES orbit crossed the Earth's shadow.

Figure 6. Radial (*R*), transverse (*T*) and normal (*W*) components of the neutral drag acceleration acting on LARES, according to the NRLMSISE-00 thermospheric density model.

Figure 7. Radial (*R*), transverse (*T*) and normal (*W*) components of the neutral drag acceleration acting on LARES, according to the GOST-2004 thermospheric density model.

Figure 8. Semi-major axis cumulative residuals of LARES determined with a precise orbit estimation over 3.7 years using GEODYN II. In one data reduction the neutral atmosphere was not considered, setting to zero the drag coefficient, while in the other data reduction the neutral atmosphere was included and the drag coefficient was a solve for parameter in the differential correction estimation process. The dramatic reduction of the semi-major axis residuals confirmed the overwhelming role played by neutral atmosphere drag in the case of LARES.

Table 1

Summary of the adjusted drag coefficients (C_D) able to reproduce the mean secular along-track non-gravitational acceleration observed on LARES.

Neutral atmosphere density model	Average adjusted drag coefficient $\langle C_D \rangle$
JR-71	3.95
MSIS-86	3.71
MSISE-90	3.73
NRLMSISE-00	3.78
GOST-2004	4.21

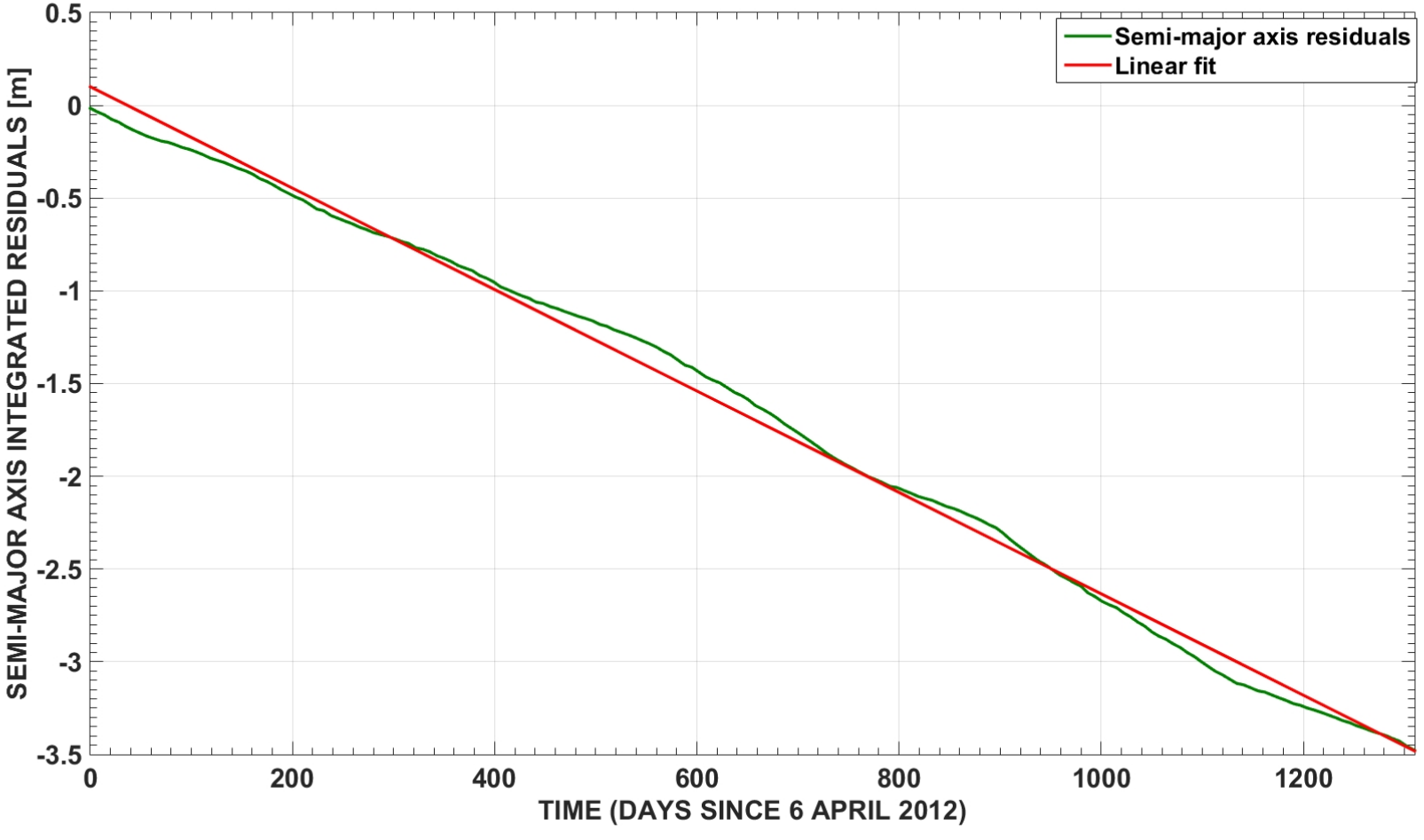
Semi-major axis residuals
Linear fit
SEMI-MAJOR AXIS INTEGRATED RESIDUALS [m]
TIME (DAYS SINCE 6 APRIL 2012)
0.5
0
-0.5
-1
-1.5
-2
-2.5
-3
-3.5
0
200
400
600
800
1000
1200

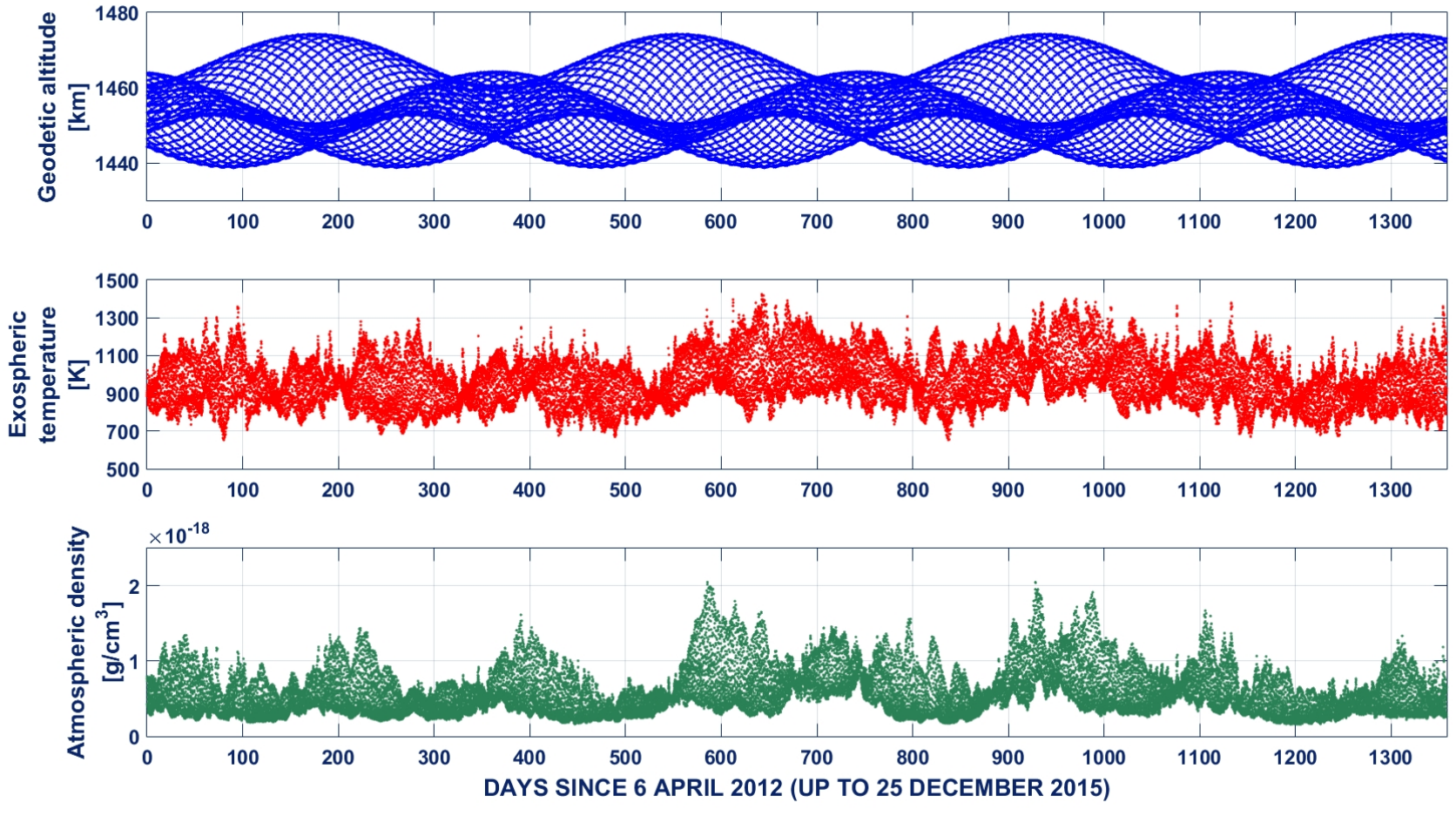
Geodetic altitude [km]
1480
1460
1440
0 100 200 300 400 500 600 700 800 900 1000 1100 1200 1300
Exospheric temperature [K]
1500
1300
1100
900
700
500
0 100 200 300 400 500 600 700 800 900 1000 1100 1200 1300
Atmospheric density [g/cm^3]
×10^-18
2
1
0
0 100 200 300 400 500 600 700 800 900 1000 1100 1200 1300
DAYS SINCE 6 APRIL 2012 (UP TO 25 DECEMBER 2015)

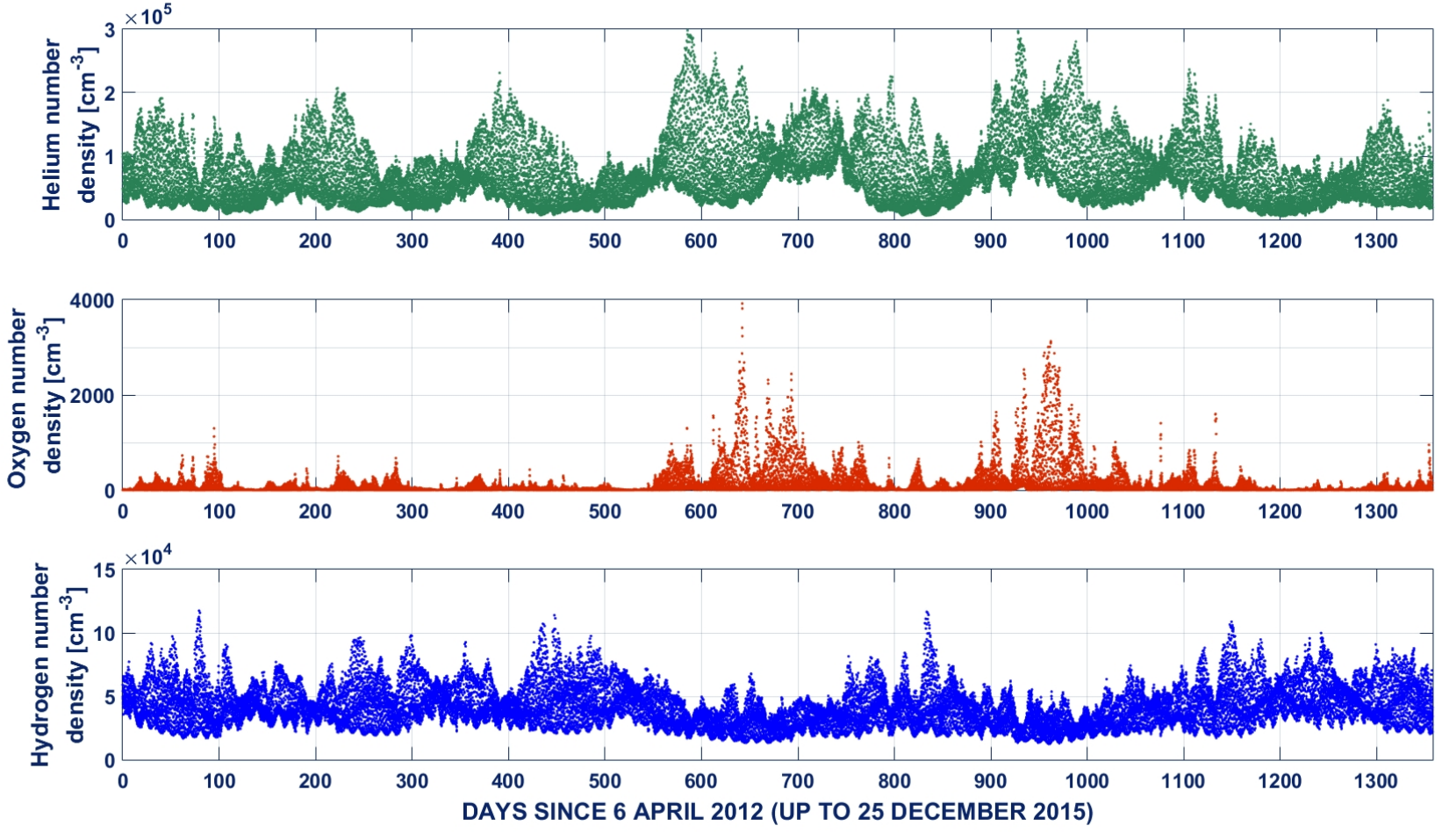
×10^5
Helium number density [cm^-3]
3
2
1
0
0
100
200
300
400
500
600
700
800
900
1000
1100
1200
1300
Oxygen number density [cm^-3]
4000
2000
0
×10^4
Hydrogen number density [cm^-3]
15
10
5
0
DAYS SINCE 6 APRIL 2012 (UP TO 25 DECEMBER 2015)

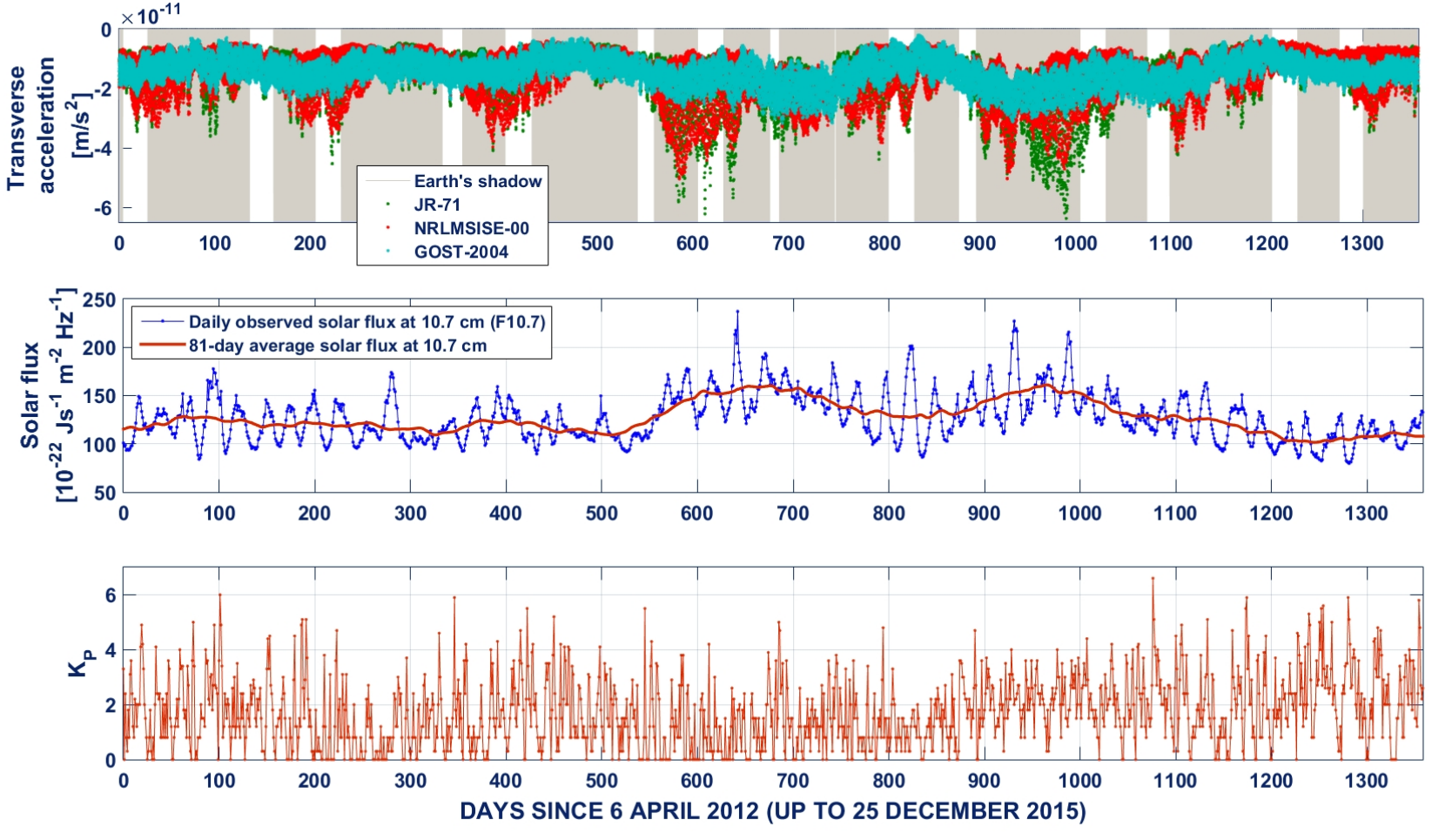
×10^-11
Transverse acceleration [m/s^2]
Earth's shadow
JR-71
NRLMSISE-00
GOST-2004
Solar flux [10^-22 Js^-1 m^-2 Hz^-1]
Daily observed solar flux at 10.7 cm (F10.7)
81-day average solar flux at 10.7 cm
K_P
DAYS SINCE 6 APRIL 2012 (UP TO 25 DECEMBER 2015)

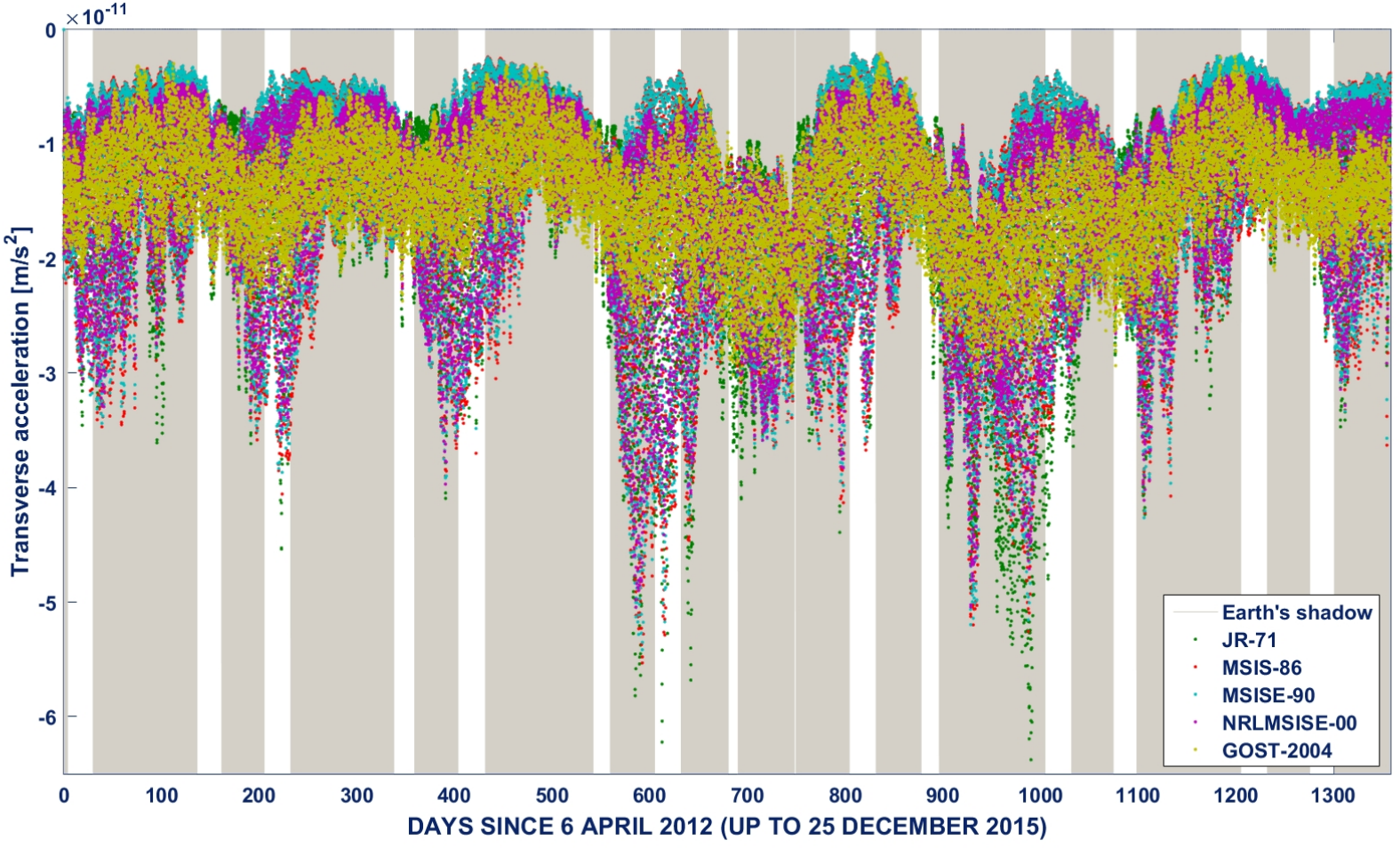
×10^-11
0
-1
-2
-3
-4
-5
-6
Transverse acceleration [m/s^2]
0
100
200
300
400
500
600
700
800
900
1000
1100
1200
1300
DAYS SINCE 6 APRIL 2012 (UP TO 25 DECEMBER 2015)
Earth's shadow
JR-71
MSIS-86
MSISE-90
NRLMSISE-00
GOST-2004

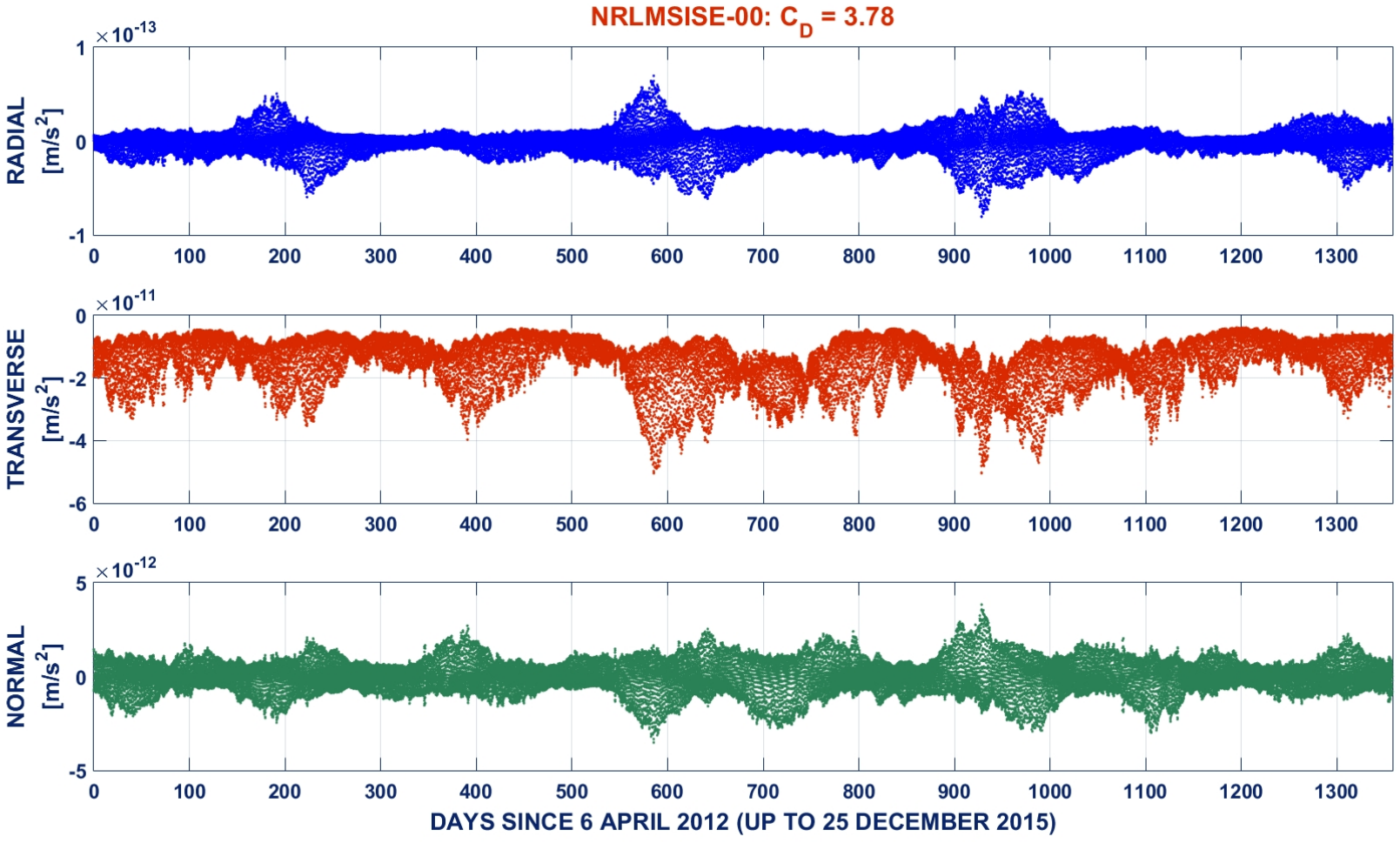
NRLMSISE-00: C_D = 3.78
RADIAL
[m/s^2]
×10^-13
1
0
-1
TRANSVERSE
[m/s^2]
×10^-11
0
-2
-4
-6
NORMAL
[m/s^2]
×10^-12
5
0
-5
0
100
200
300
400
500
600
700
800
900
1000
1100
1200
1300
DAYS SINCE 6 APRIL 2012 (UP TO 25 DECEMBER 2015)

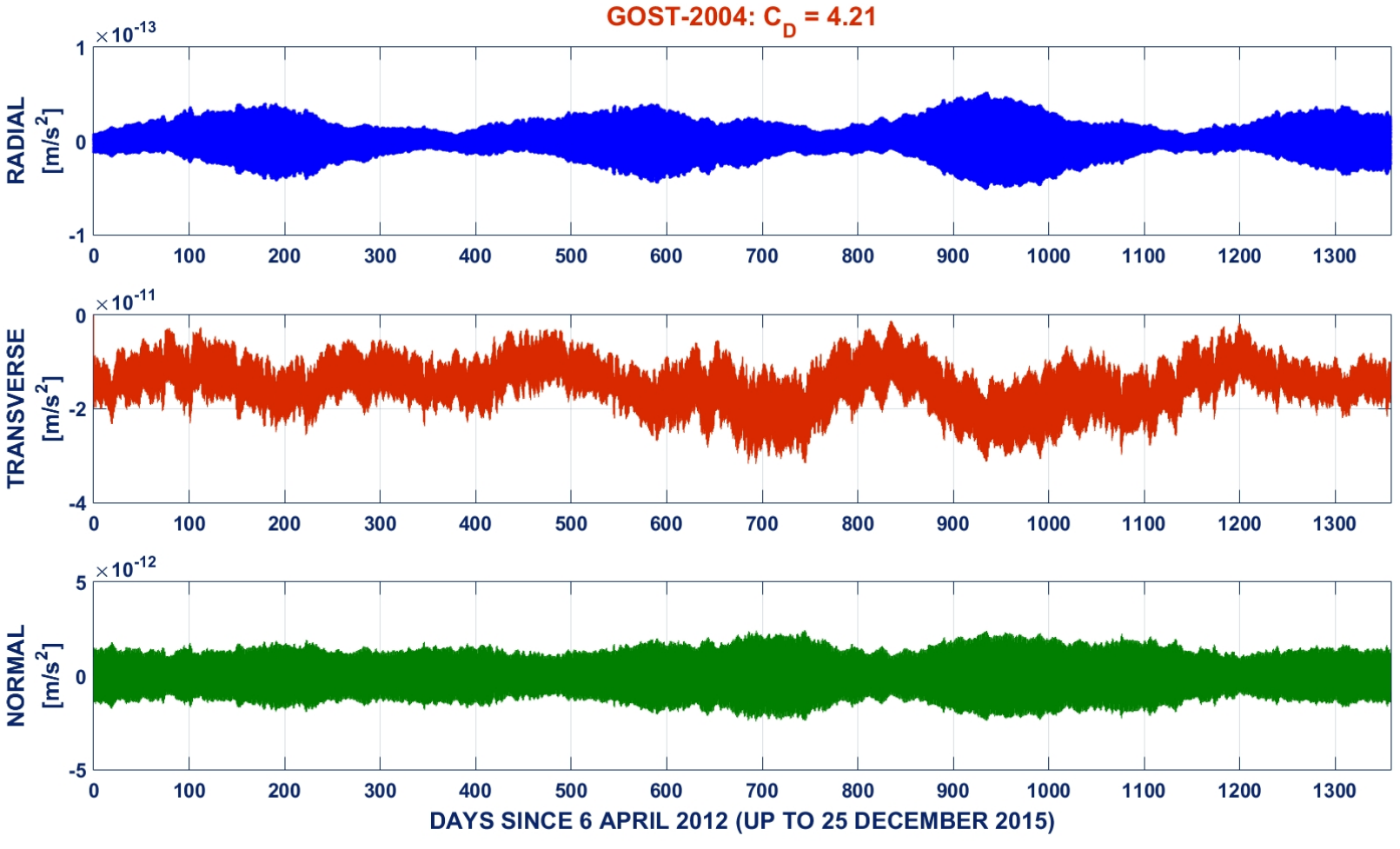
GOST-2004: C_D = 4.21
×10^-13
RADIAL
[m/s^2]
1
0
-1
×10^-11
TRANSVERSE
[m/s^2]
0
-2
-4
×10^-12
NORMAL
[m/s^2]
5
0
-5
0
100
200
300
400
500
600
700
800
900
1000
1100
1200
1300
DAYS SINCE 6 APRIL 2012 (UP TO 25 DECEMBER 2015)

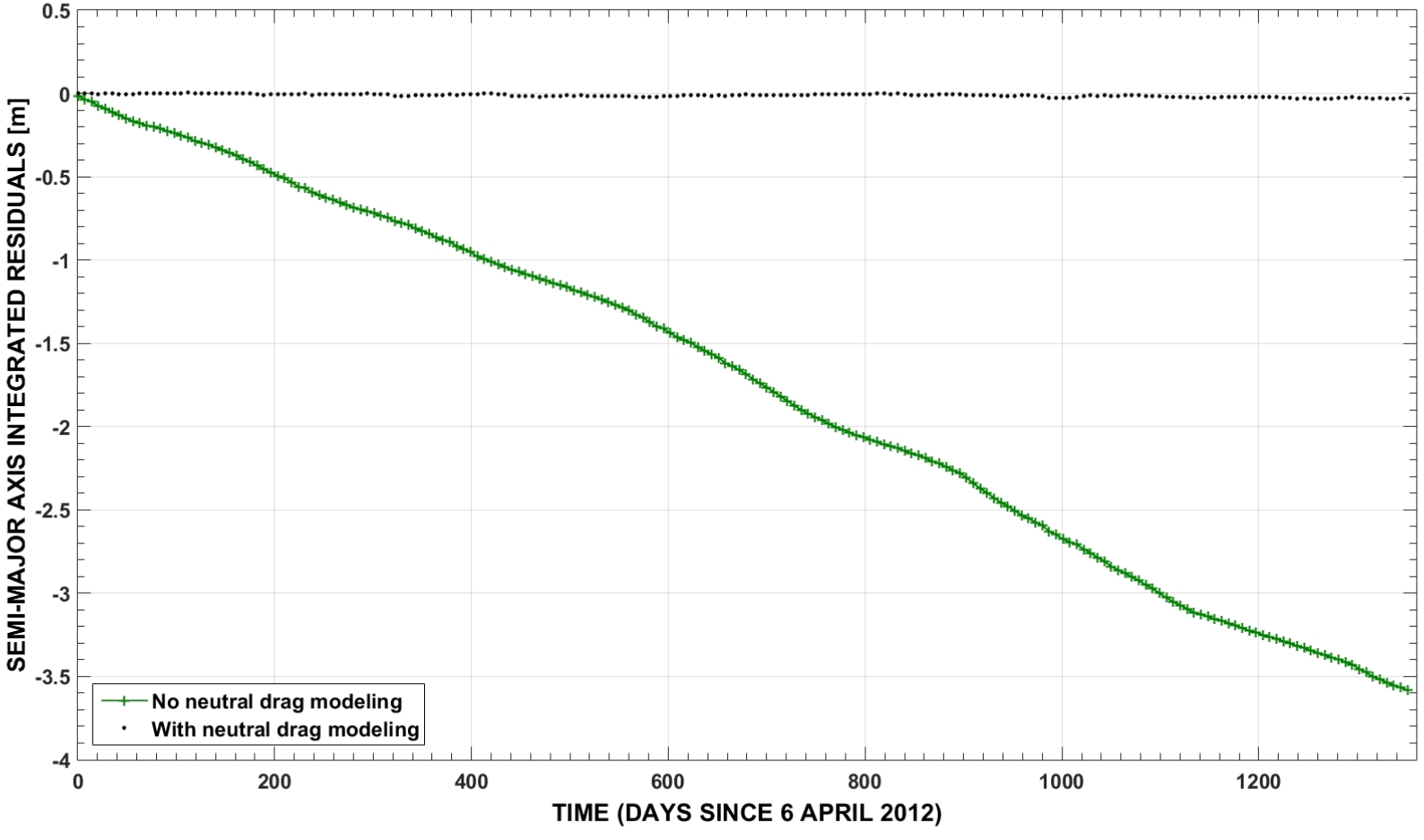
SEMI-MAJOR AXIS INTEGRATED RESIDUALS [m]
TIME (DAYS SINCE 6 APRIL 2012)
No neutral drag modeling
With neutral drag modeling
0.5
0
-0.5
-1
-1.5
-2
-2.5
-3
-3.5
-4
0
200
400
600
800
1000
1200